Labor Induction failure prediction based on B-Mode Ultrasound Image Processing using Multiscale Local Binary Patterns

Pablo Vásquez O.* †, Nestor Arana* Alberto Izaguirre*

*: Mondragon University, Mondragon, Spain
†: National University of Engineering, Managua, Nicaragua

Jorge Burgos*, Itziar Arana*

*: Obstetrics and Gynecology Service, BioCruces Health Research Institute, Bilbao, Spain

***Abstract*—Labor induction is defined as the artificial onset of labor for the purpose of vaginal birth. Cesarean section is one of the potential risks of labor induction as it occurs in about 20% of the inductions. A ripe cervix (soft and distensible) is needed for a successful labor. Changes occurring during the ripening process, will affect the interaction between cervical tissues and sound waves during ultrasound transvaginal scanning and will be perceived as gray level intensity variations in the echography image. Thus, a non-invasive method using image processing of ultrasound images may help in predicting the outcome of labor induction.**

In this paper a set of echography images from labor induction patients is analyzed using a multiscale methodology based on Local Binary Patterns and circular Gabor filters.

Results show that it is feasible to predict the outcome of a labor induction procedure using this method with a good accuracy.

Keywords-component Texture Analysis, Cervix, Local Binary Patterns

I. INTRODUCTION

Nowadays labor induction has become one of the most performed obstetric procedures. Labor induction is indicated when the maternal or fetal benefits from delivery outweigh the risks of prolonging the pregnancy. Indications for induction vary in severity and may be for medical, obstetrical or elective reasons.

Some risks related to labor induction are: cesarean section, intrapartum fetal heart rate alterations, infections, fetal acidosis, and postpartum hemorrhage. Currently in Spain about 30% of deliveries are induced and about 20% [1] end in cesarean section.

Some of these unwanted outcomes results from intervening when the uterus and cervix are not ready for labor. For this reason, the evaluation of cervical ripening is a crucial step when planning a labor induction procedure.

An accurate evaluation of cervical ripening is desirable prior labor induction process is started. It is known that the cervix tissues goes through remarkable changes along pregnancy. Collagen (about 85% of cervical microstructure) is aligned and organized in the cervix of non-pregnant women and more disorganized during remodeling of the cervix as the pregnancy progresses in preparation for the delivery [2]. Besides collagen changes, water content of the cervical tissues is also increased.

The aforementioned changes in cervical microstructure and tissue hydration are expected to be reflected on changes in the image obtained from transvaginal ultrasound since the consistency of tissues affect their interaction with the sound waves.

In this research work the potential of texture based image processing techniques in the prediction of labor induction outcomes is studied.

II. THEORETICAL BACKGROUND.

Extracting useful information from Ultrasound (US) B-mode images is a challenging task. US images are low contrast, contain blurred edges and they are normally contaminated with speckle noise. Despite these drawbacks a lot of effort has been made on processing US images. The main reason is the attractive characteristic of clinical ultrasound: a non-invasive, non-ionizing and relatively low cost medical image modality.

1) Texture

Texture is an important property of images. Although not yet formally defined in the literature, texture is related to patterns and changes on brightness in images. It has been used in many topics of image analysis. For example, it has been successfully used for segmentation of organs, e.g. liver [3], kidney [4] or for healthy and abnormal tissue classification. Successful classification examples are shown for liver [5], breast [6], or cervix [7].

One important aspect of texture is scale. It is well known that the human visual system processes images in a multi-scale way. The visual cortex has separate cells that respond to different frequencies and orientations. Analyzing texture at different resolutions is required when dealing with non-stationary textures as those obtained in medical imaging.

In a previous research it has been found that some texture parameters (mainly derived from gray level histograms and co-occurrence matrices of US cervical images) get modified depending of patients having preterm births compared to normal pregnancies [8],[9]. These findings allow us to expect a good tissue classification using texture derived parameters.

2) The Local Binary Patterns (LBP)

The LBP operator, introduced by Ojala et al. has been shown to be a powerful measure of image texture [12]. As a texture descriptor it has been found useful in many medical applications, e.g. in image segmentation [10] medical image retrieval [11] and ulcer detection [12].

In general, LBP measures the local structure at a given pixel using P samples on a circle of radius R around the pixel and summarizes this information with a unique code for each local structure or pattern. An example is shown in figure 1.

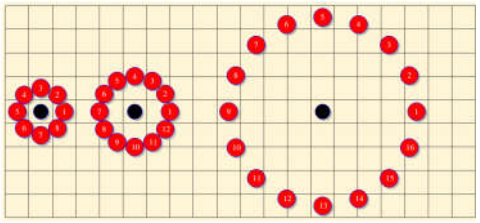

Figure 1. Different resolution LBPs using a circular neighborhood. Left P=8, R=1, Center: P=12, R=1.5$ and right P=16, R=4$.

To calculate the code, g_P, the intensity of neighboring samples is compared with the intensity of the center pixel g_C followed by a threshold operation. Each sample is thus assigned the value 1 if its gray value is larger than the threshold or the value 0 in the other case. By choosing a fixed sample position on the circle as the leading bit, the samples can be turned into a binary number. Thus each pattern has an associated unique binary number calculated using equation (1):

$$LBP_{P,R} = \sum_{p=0}^{P-1} t(g_p - g_c)2^{-p} \quad (1)$$

Sample positions on arbitrary pixel locations require interpolation. Since the original LBP was not rotation invariant the so-called rotation invariant codes were developed. Additionally there are also special patterns with at most two one-zero transitions known as uniform LBP that reduce the dimensionality of the features.

3) Co-occurrence Local Binary Patterns

In Local Binary Pattern analysis, the spatial relationship information between the LBPs is removed when generating histograms. Another method uses that spatial information by creating a Gray Level Co-occurrence Matrix (GLCM) from LBP images [13], where the authors propose using a 2D autocorrelation to generate the co-occurrence matrix.

In this paper we investigate if the inclusion of the spatial relationship improves the classification rate of the algorithm.

Instead of using the autocorrelation methodology to create the GLCM, the codes are calculated in a pointwise manner. This can be done because only points inside the predefined ROIs are processed and only a small amount of LBP codes is used. Only four neighbors are considered in the calculation (north, east, west and south) at a distance of one pixel. The GLCM is subsequently unfolded into a vector.

4) The Circular Gabor Filter

Gabor filters are constructed by combining oriented complex sinusoidal modulated by Gaussians functions. These filters have been used extensively in image processing applications such as texture segmentation and image classification.

A modified version of Gabor filters termed circular Gabor filter [14] is used here in order to study TVU images at different scales. In these filters the sinusoid varies along all orientations, leading to a circular symmetric response. These filters have been found particularly useful in rotation invariant texture analysis [15],[16]. The circular Gabor filter is defined as follows:

$$G(x,y) = \frac{1}{2\pi\sigma^2} e^{\frac{-(x^2+y^2)}{2\sigma^2}} e^{2\pi i F\left(\sqrt{x^2+y^2}\right)} \quad (2a)$$

$$F(u,v) = \frac{\sqrt{2\pi}}{2}\alpha e^{-\frac{\left(\sqrt{u^2+v^2}-F\right)^2}{2\alpha^2}} \quad (2b)$$

Where $\alpha = \frac{1}{2\pi\sigma}$. Equations 2a and 2b describe the filter in the spatial and frequency domain respectively

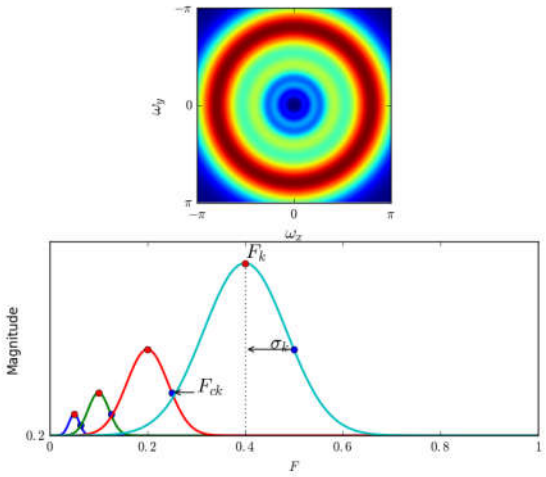

Figure 2. Frequency response of a circular Gabor filter bank using 4 scales and a section showing parameters used in the design process.

For the parameter selection we make use of the following recursive relationships (see figure 2):

$$F_k = f_o 2^{Bk}$$
$$F_{ck} = \frac{1}{2} F_k \left(2^B + 1\right) \quad (3)$$
$$\sigma_k = \frac{\lambda}{\left(F_k - F_{c(k-1)}\right)}$$

Where $\lambda = \frac{\sqrt{2\ln 2}}{2\pi}$, B is the bandwidth in octaves, F_k is the central frequency of the filter, F_{ck} is the frequency of half bandwidth and f_0 is the lower limit of the frequency range under consideration. The frequency is usually normalized by the image size N giving a maximum frequency of 0.5.

III. IMPLEMENTATION

1) *Patients and Data Collection.*

Pregnant women currently referred to the Obstetrics and Gynecology Service, BioCruces Health Research Institute (Bilbao, Spain) for labor induction, constitute our patient database for study. Inclusion criteria for this study were: singleton pregnancies, head-first presentation and ≥ 37 weeks of gestation. Pregnancies of fetus suffering from infections and abnormalities were not included. A set of 53 patients were included in this study.

Annotations about weeks of pregnancy, labor induction cause and labor outcome were also attached to the collected images. Settings for the ultrasound scanner were defined in a protocol and used by all obstetricians participating in this study. Images were acquired during routine patient transvaginal scanning prior to labor induction.

Labor induction process is usually divided into two stages: A 24 hours *ripening stage* where prostaglandins are administered, followed by an additional 12 hours *stimulation stage* where the treatment is oxytocin in case cervical ripening is not achieved.

Thus, a successful ripening is defined when a vaginal delivery was obtained within 24 hours after induction is started. Labor induction failure is considered when after 36 hours the cervix still has a Bishop Score ≤ 6.

TABLE I. PATIENTS DATABASE

	Ripening Stage (24 h)	
	Vaginal delivery	Cesarean Section
	39	4
	Stimulation stage (36 h)	
	Vaginal delivery	Cesarean Section
	5	5
Total	44	9

2) *Image Acquisition and preprocessing*

All images were acquired with a Voluson E8 Ultrasound scanner from General Electric. A total of 53 DICOM files were generated (44 belonging to patients with a vaginal delivery and 9 to cesarean section). Cases, where cesarean section was a result from causes not related to cervical ripening (breech presentation), were excluded as well as low-quality images.

All images in the database included eight ROIs. These ROIs were manually delineated by an expert obstetrician. Two of them defined the border of cervix lips (ANT, POST) and within each three inner ROIs correspond to the left (A), center (B) and right (C) portion of every lip, see figure 3. These inner ROIS were used to study if there is an optimal lip region for texture analysis as suggested in previous publications [9]

A section of 600 x 600 pixels was cropped in all the images. This sections contain the region of interest and are used to remove unwanted annotations and dark regions not carrying relevant information.

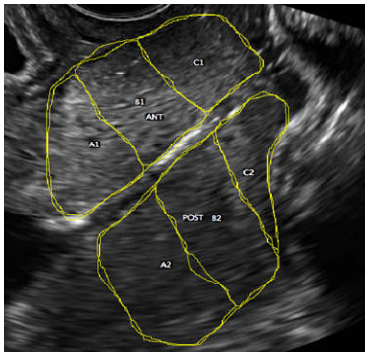

Figure 3. A sample (cropped) TVU image exhibiting the ROIs defined in this work. ANT and POST corresponds to the whole anterior and posterior lip. A, B and C define left, center and right region of every lip.

Normalization of the images was performed by the 3σ method in which all pixels in an image are restricted to be within the interval μ±3σ, where μ is the mean gray value and σ is the standard deviation. This way, gray values that may be saturated (specular reflections) or near to zero are rescaled.

3) Image processing

After the pre-processing stage, all images were filtered using a circular Gabor filter bank. For the filter bank we set $f_0 = 0.15$ and $f_{max} = 0.5$. The bandwidth B was set to one octave, i.e. 3 different scales or frequency bands for analysis were used as shown in table II.

TABLE II. FREQUENCY SCALES USED FOR FILTERING.

	F	Fc	σ
1	0.15	0.112	5
2	0.3	0.225	2.5
3	0.6	0.450	1.25

For each scale the Local Binary Pattern histogram and Co-occurrence Local Binary Pattern histogram of the selected ROIs (we considered a total of 8 ROIs, i.e. A, B, C ROIs plus ANT and POST ROIs) were calculated.

A neighborhood size of P = 8 pixels and R (Radius) = 2 pixels, were used, as well as a uniform-rotation invariant mapping which produces LBP histograms of length 10.

The histograms vectors corresponding to each image (with 2 ROIs each) are concatenated to form a single histogram vector that represent the extracted information of the image. In the case of GLCM-LBP, the LBP histogram vector and the GLCM-LBP histogram vector were concatenated. Features were further processed by normalizing each input vector individually to have unit norm.

Previous to the classification stage a feature selection step [17] was performed, where only the 60/200 (LBP/GLCM+LBP) most informative features were retained.

4) Results

For classification, two classifiers were used: a K-nearest neighbor classifier with k = 2 and a Neural Network with 20 nodes hidden layer and 2 nodes in the output layer. For these classifiers the scikit-learn Python package [18] was employed.

For the K-nearest network classifier several distance metrics such as Euclidean, CityBlock, Canberra and Minkowski were tested. The best classification results were achieved using the Canberra distance.

For the classification error, cross validation using a stratified K-fold (K=8) scheme was performed, due to the unbalanced classes. We carried out classification experiments using multiscale LBP alone and LBP +GLCM for both classifiers. ROC curves (Receiver Operator Curves, i.e. a way to analyze the optimality of the classifier), obtained in the four experiments for the best region of interest (ANT-POST) are shown in figure 4.

Among the different ROIs used in this study, the one corresponding to the whole cervical lips provides the best classification result followed by the center ROI (B1, B2). The BPNN (Back Propagation Neural Network) for this ROI selection provides an AUC (Area under the curve) score of 0.83.

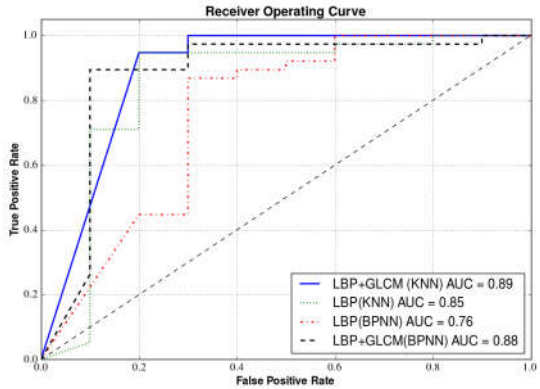

Figure 4. ROC curves and area under the curve (AUC) for the LBP and GLCM-LBP schemes using both classifiers.

In the above Figure, the diagonal dotted line represents the line of random guessing, i.e. having 50% probability of correct classification.

IV. CONCLUSION

In this paper a multiscale Local Binary Pattern methodology to the problem of assessing cervical ripening is proposed. Texture analysis of ultrasound images is not an easy task; the difference between images corresponding to the two different outcomes (vaginal and cesarean) are not distinguishable to the bare eye. By using information from different frequency bands, an improvement in accuracy of prediction is achieved compared to previous texture approaches based on local texture descriptors only.

Our results show that it is possible to differentiate, by means of image processing techniques, a ripe cervix and therefore the type of outcome from labor induction, with an accuracy of about 92 % (BPNN). This accuracy was obtained when using the whole dataset. If only the patients corresponding to the first 24 hours are included then the accuracy is reduced.

The spatial information of the LBP codes, obtained from the GLCM of the LBP image, improves the classification rate as it can be observed in the ROC curves for both classifiers and their respective AUC values.

ACKNOWLEDGMENT

The authors would like to thank to our counterparts at the Cruces University Hospital for their collaboration and advice related to clinical perspective of the provided data.

REFERENCES

[1] F. S. Molina and K. H. Nicolaides, "Ultrasound in labor and delivery," *Fetal Diagn. Ther.*, vol. 27, no. 2, pp. 61–67, 2010.

[2] H. Feltovich, K. Nam, and T. J. Hall, "Quantitative ultrasound assessment of cervical microstructure.," *Ultrason. Imaging*, vol. 32, no. 3, pp. 131–142, 2010.

[3] S. Milko, E. Samset, and T. Kadir, "Segmentation of the liver in ultrasound: a dynamic texture approach," *Int. J. Comput. Assist. Radiol. Surg.*, vol. 3, no. 1–2, pp. 143–150, 2008.

[4] C. H. Wu and Y. N. Sun, "Segmentation of kidney from ultrasound B-mode images with texture-based classification," *Comput. Methods Programs Biomed.*, vol. 84, no. 2–3, pp. 114–123, 2006.

[5] K. Krishnan, R. Sudhakar, R. K. K, R. Sudhakar, K. Krishnan, and R. Sudhakar, "Automatic Classification of Liver Diseases from Ultrasound Images Using GLRLM Texture Features," *Soft Comput. Appl.*, pp. 611–624, 2013.

[6] I. Muhimmah and R. Zwiggelaar, "Mammographic density classification using multiresolution histogram information," *Proc. Int. Spec. Top. Conf. Inf. Technol. Biomed. ITAB.*, 2006.

[7] Q. Ji, J. Engel, and E. Craine, "Texture analysis for classification of cervix lesions.," *IEEE Trans. Med. Imaging*, vol. 19, no. 11, pp. 1144–9, Nov. 2000.

[8] H. Jörn, K. Kalf, and W. Rath, "Prediction of premature birth using texture analysis of the cervix," *Ultraschall der Medizin-European J. Ultrasound*, vol. 29, no. OS2, p. PO16, 2005.

[9] T. Kuwata, S. Matsubara, N. Taniguchi, A. Ohkuchi, T. Ohkusa, and M. Suzuki, "A novel method for evaluating uterine cervical consistency using vaginal ultrasound gray-level histogram," *J. Perinat. Med.*, vol. 38, no. 5, pp. 491–494, 2010.

[10] T. Ojala and M. Pietikäinen, "Unsupervised texture segmentation using feature distributions," *Pattern Recognit.*, vol. 32, no. 3, pp. 477–486, 1999.

[11] C. Christiyana and V. Rajaman, "Comparison of Local Binary Pattern Variants for Ultrasound Kidney Image Retrieval," *Int. J. Adv. Res. Comput. Sci. Softw. Eng.*, vol. 2, no. 10, pp. 224–228, 2012.

[12] B. Li and M. Meng, "Texture analysis for ulcer detection in capsule endoscopy images," *Image Vis. Comput.*, vol. 27, no. 9, pp. 1336–1342, 2009.

[13] R. Nosaka, Y. Ohkawa, and K. Fukui, "Feature extraction based on co-occurrence of adjacent local binary patterns," *Adv. Image Video Technol.*, pp. 82–91, 2012.

[14] J. Zhang, T. Tan, and L. Ma, "Invariant texture segmentation via circular Gabor filters," *Pattern Recognition, 2002. Proceedings. 16th Int. Conf.*, vol. 2, no. 2, pp. 901–904, 2002.

[15] J. Doublet, O. Lepetit, and M. Revenu, "Contactless palmprint authentication using circular Gabor filter and approximated string matching," in *Signal and Image Processing (SIP 2007)*, 2007.

[16] L. Ma, Y. Wang, and T. Tan, "Iris recognition using circular symmetric filters," *Pattern Recognition, 2002. Proceedings. …*, 2002.

[17] S. Wang and R. M. Summers, "Machine learning and radiology," *Med. Image Anal.*, vol. 16, no. 5, pp. 933–951, 2012.

[18] F. Pedregosa, G. Varoquaux, A. Gramfort, V. Michel, B. Thirion, O. Grisel, M. Blondel, P. Prettenhofer, R. Weiss, V. Dubourg, J. Vanderplas, A. Passos, D. Cournapeau, M. Brucher, M. Perrot, and E. Duchesnay, "Scikit-learn: Machine Learning in Python," *J. Mach. Learn. Res.*, vol. 12, pp. 2825–2830, 2011.